

Preface to the Issue Dedicated to the 2002 Denali Fault Earthquake Sequence

by Charlotte Rowe, Douglas Christensen, and Gary Carver

On 3 November 2002, a M_w 7.9 earthquake, the largest continental strike-slip earthquake in North America since the 1857 Fort Tejon, California, event, occurred in central Alaska. The earthquake began with reverse faulting on a \sim 40-km extent of the previously unknown Susitna Glacier fault, but rupture transferred eastward to the right-lateral Denali fault and continued for over 200 km, finally transferring to rupture \sim 70 km of the Totschunda fault. This large, complex event we term the Denali fault earthquake (DFE), after the major crustal fault that carried most of the displacement. The initiation of the rupture, the Susitna Glacier fault, is in a remote region of central Alaska that under normal circumstances is sparsely instrumented. On 23 October of that year, however, a large earthquake of M_w 6.7, referred to as the Nenana Mountain earthquake (NME), occurred only 22 km to the west of the DFE epicenter. The NME, in hindsight recognized as a foreshock to the DFE, prompted deployment of a temporary network by the Alaska Earthquake Information Center (AEIC). Hence, the area was under significantly enhanced seismic surveillance at the time of the DFE, 10 days later, which was further augmented by the addition of 19 more stations following the DFE mainshock. As a result, high-quality data were available in the near field, providing enhanced coverage for aftershock activity from the Susitna Glacier fault initiation point, along the Denali fault as far as the western portion of the Totschunda fault, to augment regional and teleseismic data for this sequence.

As the rupture proceeded eastward, the Richardson Highway, one of the two north–south roads connecting the central and southern parts of the state, was disrupted where it crosses the Denali fault trace. Also significantly displaced was the Trans-Alaska Pipeline, operated by the Alyeska Pipeline Service Company. Remarkably, the pipeline did not rupture due in large measure to the careful design and engineering of the pipeline in the vicinity of the Denali fault. Paleoseismology and geological studies for the area suggested that an earthquake of as large as M 8.3–8.5 might occur on the Denali fault (Woodward-Clyde, 1982). In this location the pipeline was designed and constructed to withstand a \sim M 8 earthquake, with an expectation of maximum offset at this location as much as 6.1 m (20 ft) in a right-lateral sense and 1.5 m (5 ft) vertically (Cluff *et al.*, 1974); actual recorded offset during the DFE was 5.5 m laterally

and 0.8 m of vertical slip at the pipeline. Table 1 (from Cluff *et al.*, 2003) details the design criteria with respect to expected and observed maximum effects.

Ground displacements up to 8 m occurred in areas along the fault, and reported Mercalli intensities ranged from IX in the near field to II–IV (felt and associated phenomena observed) at distances up to 2000 km from the epicenter, to I (not felt but associated phenomena, such as seiches, observed) at distances over 5000 km (Hopper *et al.*, 2003). The U.S. Geological Survey (USGS) in Golden, Colorado, has compiled a large collection of reports regarding effects of this earthquake. In New Orleans, Louisiana, the water level on a lake was reported to rise and fall over a meter, and boats and docks were reported to have sustained minor damage. People in South Carolina reported observing \sim 2 cm seiches in swimming pools, and in Iowa significant turbidity was reported in wells. Closer to the epicenter, reports from Anchorage and Fairbanks, Alaska, included significant, rolling ground motion, objects falling from shelves, violent swaying of hanging items, and automobiles rocking back and forth.

Additional phenomena were observed through the effects on manufacturing and precise measurement activities throughout the continent. For example, in Ottawa, Illinois, a worker at a glass manufacturing plant reported significant shifting in the molten silica during processing operations, severely disrupting work flow. In San Antonio, Texas, a chemist was unable to use the balances for 30 to 40 min due to long-period oscillations. In Argonne, Illinois, disruptions to the particle beam source for a 1.1-km circumference particle accelerator at Argonne National Laboratory were observed for over an hour, and “made a real nice (and expensive) seismometer” for the site (“Did You Feel It” reports, USGS). Tiltmeters at an accelerator operated by Fermilab in Batavia, Illinois, recorded up to 100 microradians peak-to-peak.

Figure 1 is an isoseismal map, compiled by Margaret Hopper of the USGS, which includes all collected intensity data at this time.

We begin this volume with the results of detailed mapping and field investigation by Crone *et al.*, who document the rupture characteristics of the Susitna Glacier fault, on which rupture for the largely strike-slip DFE initiated in a M_w \sim 7.3 thrust event. This is followed by a field study of

Table 1

Comparison of Denali Fault Parameters* for Expected and Observed Earthquake Effects at the Trans-Alaska Pipeline Crossing

Denali Fault Parameters	Estimated	Design	2002 DFE
Earthquake magnitude	8.0	8.0	7.9
Horizontal acceleration at Pump Station 10	(Page, 1972) (Bolt, 1972)	0.6g	0.34g
	1.2g 0.7g		
Horizontal velocity at Pump Station 10	145 cm/sec —	74 cm/sec	114 cm/sec
Maximum right slip	9.1 m	6.1 m	Denali rupture, 8.8 m At pipeline, 5.5 m
Maximum vertical slip	2.1 m	1.5 m	Denali rupture, 2.0 m At pipeline, 0.8 m
Displacement zone width	579.1 m	610 m	Rupture within zone
Fault rupture width	76.2 m	Included	200 m

*From Cluff *et al.* (2003) (and references cited within).

Haeussler *et al.*, which documents surface slip on the Denali and Totschunda faults and the geomorphological effects observed a few days after the DFE, as well as additional observations made during follow-up field work as recently as July 2004. Macroseismic effects in Canada are presented and discussed by Cassidy and Rogers, whose data help to complete the isoseismal map provided by the USGS. Additional first-order observations are provided by Carver *et al.*, who present a detailed investigation of tree damage in the vicinity of the Denali fault, as well as compelling evidence that the large ($M \sim 7.3$) 1912 event of central Alaska, whose seismologically determined epicenter has large uncertainties due to poor records, also arose due to failure on the Denali fault. David Boore presents a study of site response in Anchorage, using data from permanent strong- and weak-motion networks in the Anchorage area, and derives response spectra that will be important for future earthquake engineering efforts for the city, which is situated in part atop deposits that fall within National Earthquake Hazard Reduction Program (NEHRP) site classes C and D.

From geological, dendrochronological, macroseismic, and engineering considerations, we then move to geophysical profiles of the Denali fault, historic seismicity, and seismotectonics. Brocher *et al.* present an analysis of crustal seismic velocity structure in the vicinity of the Denali fault, using seismic refraction and reflection data recorded during the 1986–1987 Trans-Alaska Crustal Transect (TACT). Fisher *et al.* combine their interpretation of the TACT seismic reflection profile with magnetotelluric, magnetic, and gravity data to investigate additional constraints on crustal seismic models for the area. Diane Doser presents a detailed study of historic seismicity between 1912 and 1988 to examine stress changes preceding the 2002 DFE. Charles Bufe investigates the effects of Coulomb stress transfer to the Denali fault and other area faults, following the 1964 Prince William Sound M_w 9.2 earthquake. Ratchkovski *et al.* investigate spatial and temporal variations in seismicity and stress orientation immediately prior to and during the DFE and its aftershock sequence.

The next set of articles deals with slip and rupture modeling based on various complementary observations. Wright

et al. use InSAR interferograms combined with campaign and continuous GPS sites to determine the geometry of the Susitna Glacier fault and to develop a slip model for the DFE sequence. Aagard *et al.* use three-dimensional spontaneous dynamic rupture models to investigate the rupture on the Susitna Glacier fault and nearly simultaneous rupture on the Denali fault. Bhat *et al.* analyze dynamic slip transfer from the Denali fault to the Totschunda fault using two-dimensional numerical simulations. Oglesby *et al.* perform inverse kinematic models using local seismic and GPS data, in combination with forward dynamic models, to investigate the complex rupture process of the DFE. Art Frankel investigates the rupture process using displacement waveforms and high-frequency acceleration envelopes, finding not only subevents in agreement with those detected by other researchers, but also evidence in support of super-shear rupture. Dunham and Archuleta model the acceleration of rupture to super-shear velocities using elastodynamic considerations to demonstrate that initial pulses arise from supershear stress release on the fault, whereas later, fault-normal pulses are due to trailing slip propagating at subshear speeds.

Choy and Boatwright analyze teleseismic P and SH waves to determine the DFE rupture characteristics and to identify similar slip pulse (subevent) features, and they also note significant rupture directivity as well as portions of energy-deficient rupture, which has implications for seismic hazard for large strike-slip events. Ozacar and Beck compare the DFE to the 2001 Kunlun fault earthquake in Mongolia, observing many common features including unilateral rupture, high rupture velocities, and similar source complexity. Velasco *et al.* investigate the strong rupture directivity of the DFE using surface-wave displacement seismograms.

The strong directivity of the DFE is thought to be a significant contributor to the many, significant examples noted of remote earthquake triggering. In the aftermath of the passage of large Love and Rayleigh waves from the DFE, earthquakes were triggered at distances of over 3000 km from the epicenter. This is the greatest distance documented to date of dynamic triggering, and we close this special issue with a collection of articles that present triggering effects in Alaska, Washington, Idaho, Montana, Yellowstone (Wyo-

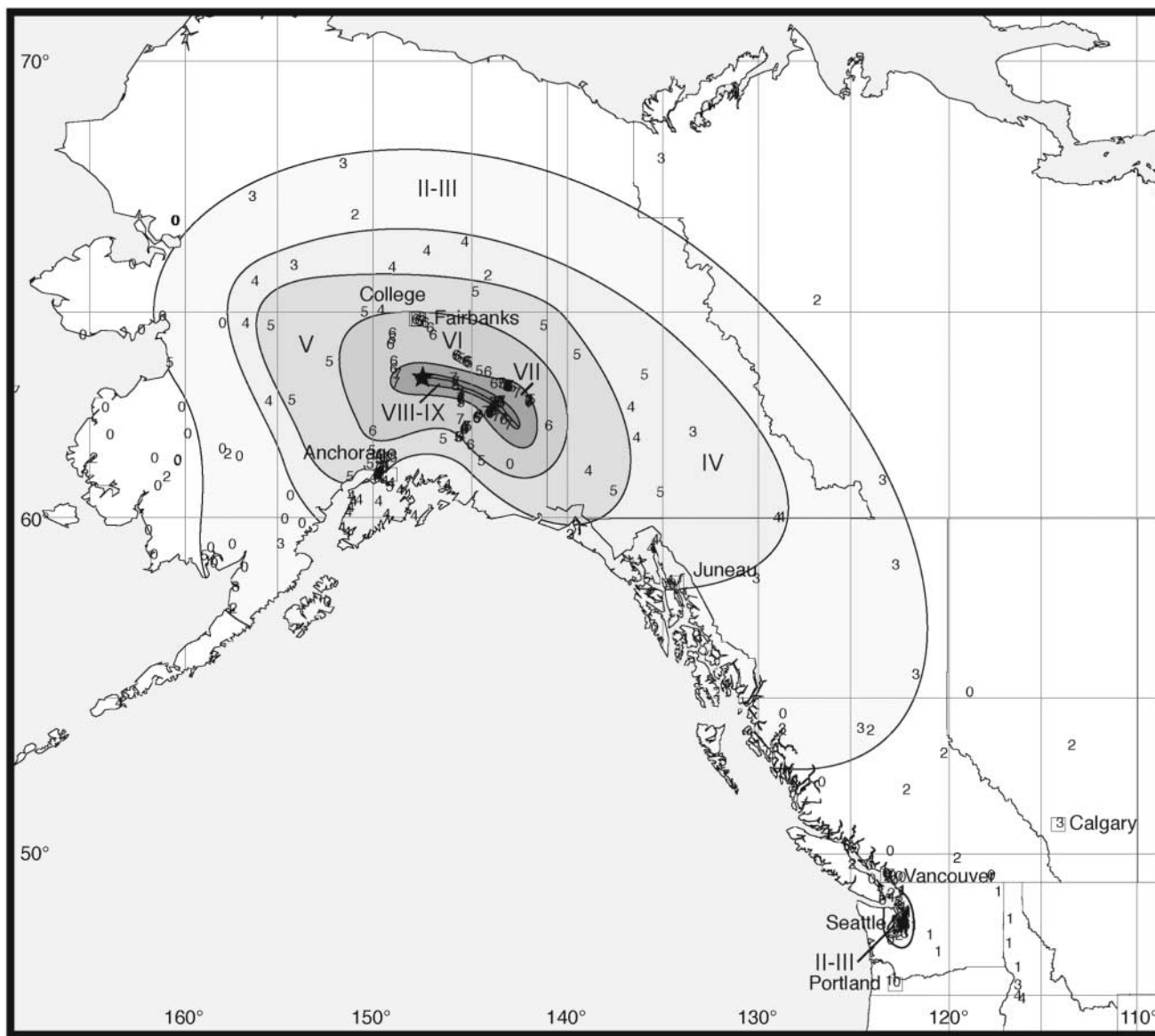


Figure 1. Isoseismal map for the 3 November 2002 DFE (provided by Margaret Hopper, USGS). Numbers on the map represent Modified Mercalli intensities assigned to the sites based on data from the Community Internet Intensity Map (“Did You Feel It?”) Web site contributed by David J. Wald, a field survey in the epicentral region by Artak H. Martirosyan, a postal canvass, information from John Cassidy of the Geological Survey of Canada, and press and other reports. A “0” on the map represents a report that the earthquake was not felt at that location; a “1” on the map represents a report of an observed earthquake effect (for example, a seiche or swinging objects) from a location where the earthquake was not felt. Isoseismal intensities are denoted by Roman numerals. A star indicates the epicenter, and the line within the VII-IX isoseismal shows the rupture.

ming), Utah, and Long Valley/Mammoth Mountain (California).

Moran *et al.* discuss triggering at the Katmai volcanic group in Alaska and the lack of triggering at other instrumented volcanic/geothermal sites in the state. Husker and Brodsky investigate triggered seismicity in Idaho and Montana and consider different geological discriminants to com-

pare possible mechanisms. Husen *et al.* document significant triggering effects at Yellowstone (Wyoming) and compare the triggered behavior to ordinary swarm activity within, and near, the caldera. Triggering in Utah is discussed by Pankow *et al.*, in the context of large dynamic stresses arising from the significant directivity of the DFE. The Utah triggered events provide a clear case that dynamic triggering can be

vigorous in areas where geothermal and volcanic influences are not present. In contrast to the Utah triggering, most activity triggered in California and the Pacific Northwest was recorded in areas of known volcanic and/or geothermal activity. Prejean *et al.* document earthquake triggering at Mount Rainier (Washington), Geysers and Coso geothermal fields (California), and Long Valley/Mammoth Mountain (California). Johnston *et al.* investigate deformational offsets recorded by strainmeters at Long Valley and compare deformation moment to cumulative seismic moment of the associated seismicity. Finally, Sánchez and McNutt document instances at two Alaska volcanoes where the dynamic effect of the DFE appears to inhibit, rather than trigger, seismicity, and they speculate on the physical scenarios which may explain the seismic decline.

Many of the articles in this volume are augmented with electronic supplements, ranging from photographic collections showing near-fault effects observed during field investigation to mpeg movie files of modeled dynamic rupture propagation. We encourage readers to take the time to visit the sites indicated for these supplements, as they provide valuable enhancements to their associated articles.

We hope that the collected articles in this volume will advance both theoretical and practical efforts toward understanding not only the near- and far-field effects, but also the hazards associated with large, strike-slip earthquakes such as the DFE, arising from complex sources involving significant slip transfer across multiple faults. In particular, the DFE has spotlighted the importance of conservative application of seismic design criteria in the building of critical infrastructure through the successful prevention of an environmental (and economic) catastrophe related to the effects on the Trans-Alaska Pipeline.

Acknowledgments

We wish to thank all the authors who contributed to this volume, and we extend a special thanks to the many reviewers who provided helpful and insightful reviews for the included articles, sometimes under rather tight

time constraints. Macroseismic information presented in this introduction was collected and compiled by Margaret Hopper of the USGS. Additional help in obtaining related information was provided by David Wald and Trilby Cox. Pipeline design information was obtained through the help of Jim Roddick, Marcia McLaren, and Lloyd Cluff. We also appreciate the helpful review comments offered by A. Michael (BSSA editor) and the invaluable efforts of Carol Mark (managing editor) and Stephanie Hansen (editorial assistant).

References

- Cluff, L. S., D. B. Slemmons, G. E. Brogan, and M. K. Koringa (1974). Summary report, basis for pipeline design for active fault crossings for the Trans-Alaska Pipeline System, prepared for Alyeska Pipeline Service Company by Woodward-Lundgren and Associates, 1257 pp.
- Cluff, L. S., R. A. Page, D. B. Slemmons, and C. B. Crouse (2003). Seismic hazard exposure for the Trans-Alaska pipeline, in *Proceedings of the Sixth U.S. Conference on Lifeline Earthquake Engineering*, ASCE Technical Council on Lifeline Earthquake Engineering, Long Beach, Calif., 535–546.
- Hopper, M. G., J. W. Dewey, and D. J. Wald (2003). Intensity distribution and isoseismal maps for the Denali, Alaska, earthquake of 3 November 2002, *EOS*, **84**, (Fall Meet. Suppl.), abstract S12A-0373.
- Woodward-Clyde Consultants (1982). Development and Initial Application of Software for Seismic Exposure Evaluation Volume II, report prepared for the National Oceanic and Atmospheric Administration, San Francisco.

Los Alamos National Laboratory
EES-11, MS D-408
Los Alamos, New Mexico 87545
char@lanl.gov
(C.R.)

Geophysical Institute
University of Alaska
Fairbanks, Alaska 99775
doug@giseis.alaska.edu
(D.C.)

Carver Geologic, Inc.
P.O. Box 52
12021 Middlebay Drive
Kodiak, Alaska 99615
egeol@alaska.com
(G.C.)

Manuscript received 28 September 2004.